Title

Path planning with Pythagorean-hodograph curves for unmanned or autonomous vehicles

Journal

Proceedings of the Institution of Mechanical Engineers Part G Journal of Aerospace Engineering, 232(7)

ISSN

0954-4100

Authors

Farouki, Rida T
Giannelli, Carlotta
Mugnaini, Duccio
et al.

Publication Date

2018-06-01

DOI

10.1177/0954410017690550

Peer reviewed

Path planning with Pythagorean-hodograph curves for unmanned or autonomous vehicles

Rida T. Farouki
Department of Mechanical and Aerospace Engineering,
University of California, Davis, CA 95616, USA.

Carlotta Giannelli,
Dipartimento di Matematica e Informatica "U. Dini,"
Università di Firenze, Viale Morgagni 67/A, I–50134 Firenze, Italy.

Duccio Mugnaini,
Dipartimento di Scienze e Alta Tecnologia,
Università dell'Insubria, Viale Vallegio 11, I–22100 Como, Italy.

Alessandra Sestini
Dipartimento di Matematica e Informatica "U. Dini,"
Università di Firenze, Viale Morgagni 67/A, I–50134 Firenze, Italy.

Abstract

The Pythagorean–hodograph (PH) curves offer distinct advantages in planning curvilinear paths for unmanned or autonomous air, ground, or underwater vehicles. Although several authors have discussed their use in these contexts, prior studies contain misconceptions about the properties of PH curves or invoke heuristic approximate constructions when exact methods are available. To address these issues, the present study provides a basic introduction to the key properties of PH curves, and describes some exact constructions of particular interest in path planning. These include (1) maintenance of minimum safe separations within vehicle swarms; (2) construction of paths of different shape but identical arc length, ensuring simultaneous arrival of vehicles travelling at a constant speed; (3) determination of the curvature extrema of PH paths, and their modification to satisfy a given curvature bound; and (4) construction of curvature–continuous paths of bounded curvature through fields of polygonal obstacles.

Keywords: path planning, unmanned vehicles, autonomous vehicles, obstacle avoidance, safe separation, simultaneous arrival, curvature extrema, Pythagorean–hodograph curves.

e–mail addresses: farouki@ucdavis.edu, carlotta.giannelli@unifi.it, dmugnaini@uninsubria.it, alessandra.sestini@unifi.it

1 Introduction

Many authors have recently proposed the use of *Pythagorean–hodograph* (PH) *curves* in the context of path planning for autonomous or remotely–operated aerial, land, or submarine vehicles, such as unmanned aerial vehicles (UAVs) or autonomous underwater vehicles (AUVs): see [2, 4, 5, 6, 18, 20, 21, 22, 23, 24, 25, 26, 28, 29, 30, 31]. Feasible paths must satisfy various constraints, such as bounds on the path curvature or climb angle, avoidance of environmental obstacles, and maintenance of safe separations in vehicle swarms.

The PH curves were introduced in [16] to facilitate *exact* computations of basic geometrical properties that require numerical approximations in the context of general polynomial curves (see [10] for a comprehensive treatment). These properties have been extensively and systematically exploited in the context of computer numerical control (CNC) manufacturing systems [13]. The existing autonomous vehicle path planning literature, on the other hand, embodies several misconceptions concerning PH curves, and does not fully exploit their advantageous properties and existing capabilities.

For example, it has been claimed [20, 23, 24, 25, 28, 31] that the PH curves possess a "uniform distribution of points on the curve" or "uniformity in the parametric distribution" [25] and this "contributes to the smoothness of the path" [23, 24, 25]. A "uniform distribution of points" has also been claimed [28] for the offsets to planar PH curves. However, these claims are incorrect. The parametric speed $\sigma(\xi) = |\mathbf{r}'(\xi)|$ of a curve $\mathbf{r}(\xi)$ is the derivative $\mathrm{d}s/\mathrm{d}\xi$ of arc length s with respect to the parameter ξ. For a polynomial curve, other than a straight line, $\sigma(\xi)$ cannot be constant since $|\mathbf{r}'(\xi)| \to \infty$ as $|\xi| \to \infty$ if $\mathbf{r}(\xi)$ is not a straight line. It is a much more subtle matter [17] that this is

also true of rational curves. Moreover, smoothness is an intrinsic geometrical property, that is independent of parameterization uniformity.

Although uniform (i.e., arc–length) polynomial and rational curved path parameterizations paths are impossible, the PH curves come nearest to this unattainable ideal since their arc lengths are defined[1] by monotone–increasing polynomial functions $s(\xi)$ in the curve parameter. Thus, for a given distance s_* along a PH curve, one can compute the corresponding curve parameter ξ_* — and hence the curve point $\mathbf{r}(\xi_*)$ — to machine precision, as the unique real root of the equation $s(\xi_*) - s_* = 0$ by a few Newton–Raphson iterations. This property is useful for real–time execution of curved paths at constant or variable speed [13] and can be used to accurately assess maintenance of safe separations between multiple autonomous vehicles. It is also possible to construct multiple paths of precisely equal arc length.

The intent of this paper is to (1) summarize the construction, properties, and applications of the PH curves, and dispel some common misconceptions concerning them; (2) describe an open–source software library incorporating some basic construction and analysis functions for planar PH curves; and (3) introduce some novel PH curve utilities that are of particular interest in the path planning problem for multiple autonomous vehicles.

The focus of this study is on geometrical and kinematical considerations in path planning. Although vehicle dynamical limitations are not explicitly considered at present, path geometry and kinematics are of direct relevance

[1] Only *polynomial* PH curves are considered here: *rational* PH curves do not (in general) have rational arc lengths, since the integrals of rational functions may incur transcendental terms. The focus is on *regular* curves, with $\mathbf{r}'(\xi) \neq \mathbf{0}$ for all ξ (see [10] for further details).

in ensuring physically realizable trajectories. For example, at a specified fixed speed, the path curvature must be bounded to ensure compatibility with the maximum vehicle steering rate, and path inclination with the horizontal must be consistent with the maximum climb rate of the vehicle.

The remainder of this paper is organized as follows. First, the definitions, constructions, and key properties of planar PH curves are briefly described in Section 2, based on the complex–number representation. Section 3 then summarizes an existing open–source software library for the construction and analysis of planar PH quintics, that can be exploited in the path planning context. Some representative applications of PH curves are then addressed: the maintenance of safe separations within swarms of autonomous vehicles in Section 4; the construction of families of curved paths with identical arc lengths, ensuring the simultaneous arrival of multiple autonomous vehicles travelling at constant speed in Section 5; the imposition of path curvatures consistent with vehicle steering rates in Section 6; and curvature–continuous rounding of sharp corners in piecewise–linear paths through a field of polygon obstacles in Section 7. Finally, Section 8 summarizes the key results of this study, and suggests directions for further investigation.

2 Planar Pythagorean-hodograph curves

For brevity, the focus of this study will be on planar Pythagorean–hodograph (PH) curves, based on the complex–number representation [8]. Many of the results can be extended to the case of paths specified by spatial PH curves, using the quaternion representation (see [10] for further details).

A plane polynomial PH curve $\mathbf{r}(\xi) = (x(\xi), y(\xi)), \xi \in [\,0, 1\,]$ has derivative components $x'(\xi), y'(\xi)$ that satisfy [16] the condition

$$x'^2(\xi) + y'^2(\xi) \;=\; \sigma^2(\xi) \tag{1}$$

for some polynomial $\sigma(\xi)$, which specifies the *parametric speed* of $\mathbf{r}(\xi)$ — i.e., the derivative of the arc length s with respect to the curve parameter ξ. This feature endows PH curves with many attractive computational properties — they have rational unit tangents, normals, curvatures, and offset curves; their arc lengths are exactly computable; and they are particularly well suited to real–time precision motion control applications [10].

For a primitive curve, with $\gcd(x'(\xi), y'(\xi)) = \text{constant}$, a sufficient and necessary condition for satisfying (1) is that $x'(\xi), y'(\xi)$ must be expressible in terms of polynomials $u(\xi), v(\xi)$ with $\gcd(u(\xi), v(\xi)) = \text{constant}$ in the form

$$x'(\xi) \;=\; u^2(\xi) - v^2(\xi)\,, \quad y'(\xi) \;=\; 2\,u(\xi)v(\xi)\,.$$

This structure is embodied in the complex representation, wherein a PH curve of degree $n = 2m+1$ is generated [8] from a degree–m complex "pre–image" polynomial

$$\mathbf{w}(\xi) \;=\; u(\xi) + \mathrm{i}\,v(\xi) \;=\; \sum_{k=0}^{m} \mathbf{w}_k \binom{m}{k} (1-\xi)^{m-k}\xi^k \tag{2}$$

with Bernstein coefficients $\mathbf{w}_k = u_k + \mathrm{i}\,v_k$ by integration of the expression

$$\mathbf{r}'(\xi) \;=\; \mathbf{w}^2(\xi)\,. \tag{3}$$

The parametric speed, unit tangent, and curvature of $\mathbf{r}(\xi)$ may be formulated [8] in terms of $\mathbf{w}(\xi)$ as

$$\sigma(\xi) \;=\; |\mathbf{w}(\xi)|^2\,, \quad \mathbf{t}(\xi) \;=\; \frac{\mathbf{w}^2(\xi)}{\sigma(\xi)}\,, \quad \kappa(\xi) \;=\; 2\,\frac{\mathrm{Im}(\overline{\mathbf{w}}(\xi)\mathbf{w}'(\xi))}{\sigma^2(\xi)}\,. \tag{4}$$

Since $\sigma(\xi)$ is a polynomial of degree $2m$, the cumulative arc length function

$$s(\xi) \;=\; \int_0^{\xi} \sigma(\tau)\,\mathrm{d}\tau$$

is likewise just a polynomial in ξ, of degree $2m+1$.

The simplest planar PH curves that can inflect, and have shape freedoms similar to those of "ordinary" cubics, are the quintics. A planar PH quintic is defined by choosing a quadratic polynomial $\mathbf{w}(\xi)$, with Bernstein coefficients $\mathbf{w}_0, \mathbf{w}_1, \mathbf{w}_2$. On integrating (3), the Bézier control points $\mathbf{p}_k = x_k + \mathrm{i}\, y_k$ of the resulting PH quintic

$$\mathbf{r}(\xi) \;=\; \sum_{k=0}^{5} \mathbf{p}_k \binom{5}{k} (1-\xi)^{5-k} \xi^k$$

may be expressed [8] as

$$\begin{aligned}
\mathbf{p}_1 \;&=\; \mathbf{p}_0 + \frac{1}{5}\,\mathbf{w}_0^2\,, \\
\mathbf{p}_2 \;&=\; \mathbf{p}_1 + \frac{1}{5}\,\mathbf{w}_0\mathbf{w}_1\,, \\
\mathbf{p}_3 \;&=\; \mathbf{p}_2 + \frac{1}{5}\,\frac{2\mathbf{w}_1^2 + \mathbf{w}_0\mathbf{w}_2}{3}\,, \\
\mathbf{p}_4 \;&=\; \mathbf{p}_3 + \frac{1}{5}\,\mathbf{w}_1\mathbf{w}_2\,, \\
\mathbf{p}_5 \;&=\; \mathbf{p}_4 + \frac{1}{5}\,\mathbf{w}_2^2\,,
\end{aligned} \tag{5}$$

where $\mathbf{p}_0$ is a free integration constant. The parametric speed polynomial

$$\sigma(\xi) \;=\; \sum_{k=0}^{4} \sigma_k \binom{4}{k} (1-\xi)^{4-k} \xi^k \tag{6}$$

has the Bernstein coefficients

$$\begin{aligned}
\sigma_0 \;&=\; |\mathbf{w}_0|^2\,, \quad \sigma_1 \;=\; \mathrm{Re}(\overline{\mathbf{w}}_0\mathbf{w}_1)\,, \\
\sigma_2 \;&=\; \frac{2|\mathbf{w}_1|^2 + \mathrm{Re}(\overline{\mathbf{w}}_0\mathbf{w}_2)}{3}\,, \\
\sigma_3 \;&=\; \mathrm{Re}(\overline{\mathbf{w}}_1\mathbf{w}_2)\,, \quad \sigma_4 \;=\; |\mathbf{w}_2|^2\,.
\end{aligned}$$

Correspondingly, the Bernstein form

$$s(\xi) \;=\; \sum_{k=0}^{5} s_k \binom{5}{k} (1-\xi)^{5-k} \xi^k \tag{7}$$

of the arc length polynomial is specified by the coefficients

$$s_0 \;=\; 0 \qquad \text{and} \qquad s_k \;=\; \frac{1}{5} \sum_{j=0}^{k-1} \sigma_j \,, \quad k = 1, \ldots, 5 \tag{8}$$

and the total arc length is

$$S \;=\; s(1) \;=\; s_5 \;=\; \frac{\sigma_0 + \sigma_1 + \sigma_2 + \sigma_3 + \sigma_4}{5} \,. \tag{9}$$

Based on the complex representation, algorithms for the construction and analysis of planar PH curves have reached a mature state of development — for example, see [11, 12, 14] and Section 3 below.

3 Open-source `PHquintic` software library

An open–source library of key functions for the construction and analysis of planar PH quintic curves has been developed in the `C` programming language [7]. The complex–number representation was employed to facilitate compact and efficient implementations. Each PH quintic segment $\mathbf{r}(\xi)$ is defined by a data structure that incorporates complex arrays specifying the Bézier control points $\mathbf{p}_0, \ldots, \mathbf{p}_5$ and the coefficients $\mathbf{w}_0, \mathbf{w}_1, \mathbf{w}_2$ of the pre–image polynomial, and real arrays for the coefficients $\sigma_0, \ldots, \sigma_4$ and $s_0, \ldots, s_5$ of the parametric speed and arc length polynomials. These data are redundant, but their pre–computation helps to improve the efficiency of subsequent computations, and circumvents possible inconsistencies. The functions currently available in the `PHquintic` library are as follows.

- `construct_PHquintic`: for given initial and final pairs of control points $\mathbf{p}_0, \mathbf{p}_1$ and $\mathbf{p}_4, \mathbf{p}_5$ this function "fills in" the two interior points $\mathbf{p}_2, \mathbf{p}_3$ so as to generate a PH quintic segment $\mathbf{r}(\xi)$, $\xi \in [\,0, 1\,]$. This amounts to solving a first–order Hermite interpolation problem, with four distinct formal solutions [14]. The function returns the "good" solution, having the least value of the absolute rotation index $R_{\mathrm{abs}} = \int |\kappa| \, \mathrm{d}s$.

- `open_PHquintic_spline` and `closed_PHquintic_spline`: for a given sequence of $N + 1$ points $\mathbf{q}_0, \ldots, \mathbf{q}_N$ in the plane, these two functions compute C^2 piecewise PH quintic spline curves interpolating $\mathbf{q}_0, \ldots, \mathbf{q}_N$ as nodal points. An efficient Newton–Raphson iteration, commencing with an accurate starting approximation, ensures rapid convergence to the solution of the non–linear equations governing the PH quintic spline construction [12]. The "open" splines employ cubic end spans, while the "closed" splines (with $\mathbf{q}_N = \mathbf{q}_0$) use periodic end conditions.

- `PHquintic_energy`: this function provides an exact computation of the bending energy integral $\int \kappa^2 \, \mathrm{d}s$ for a single PH quintic curve segment, based on a complex partial fraction expansion of the integrand [9].

- `PHquintic_offset`: for a given PH quintic segment $\mathbf{r}(\xi)$ and a (signed) offset distance d, this function returns the control point homogeneous coordinates (W_k, X_k, Y_k), $k = 0, \ldots, 9$ that exactly define [16] the offset curve $\mathbf{r}_d(\xi) = \mathbf{r}(\xi) + d\,\mathbf{n}(\xi)$, where $\mathbf{n}(\xi)$ is the unit normal to $\mathbf{r}(\xi)$.

4 Maintenance of minimum separations

For brevity, this study deals primarily with vehicles travelling at a prescribed constant speed. However, a key advantage of the PH curves is the ability to specify continuously–variable speeds along curved paths — as functions of time, path arc length, curvature, etc. This capability has been demonstrated in the context of real–time motion control of CNC machines [13].

Consider the problem of determining whether the traversal of two planar PH quintic paths $\mathbf{r}(\mu)$, $\mu \in [\,0,1\,]$ and $\mathbf{s}(\nu)$, $\nu \in [\,0,1\,]$ at a constant speed V will incur a close approach with separation less than a safe minimum distance δ. If $p(\mu)$ and $q(\nu)$ are the polynomial arc length functions for $\mathbf{r}(\mu)$ and $\mathbf{s}(\nu)$, and the motions start at $\mathbf{r}(0)$ and $\mathbf{s}(0)$ at time $t = 0$, this amounts to identifying if parameter values $(\mu, \nu) \in [\,0,1\,]^2$ exist, such that

$$p(\mu) \;=\; q(\nu) \qquad \text{and} \qquad |\,\mathbf{r}(\mu) - \mathbf{s}(\nu)\,| \;<\; \delta\,.$$

Geometrically, this corresponds to asking whether the value of the bivariate function $d(\mu,\nu) = |\,\mathbf{r}(\mu) - \mathbf{s}(\nu)\,|$, restricted to the degree 5 algebraic curve defined by the equation $f(\mu,\nu) = p(\mu) - q(\nu) = 0$, dips below δ.

In general, this problem has no closed–form solution, but the polynomial nature of $p(\mu)$ and $q(\nu)$ allows an essentially exact test for a maintenance of the safe closest–approach threshold δ for any specified sampling distance Δs (corresponding to a sampling time $\Delta t = \Delta s/V$) along the paths. Namely, if μ_k, ν_k (≤ 1) are the unique real roots of the equations

$$p(\mu_k) \;=\; q(\nu_k) \;=\; k\Delta s\,, \quad k = 0, 1, 2, \ldots$$

the distance at time $t_k = k\Delta t$ is $\delta_k = |\,\mathbf{r}(\mu_k) - \mathbf{s}(\nu_k)\,|$. For modest Δs values

μ_k, ν_k are good estimates of μ_{k+1}, ν_{k+1} so the latter can be accurately and efficiently computed from the former by a few Netwon–Raphson iterations.

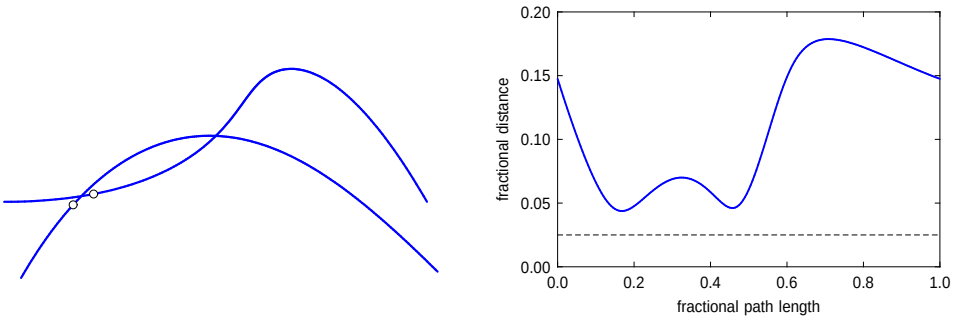

Figure 1: Left: two planar PH quintic paths of equal arc length traversed at constant speed, with the points of closest approach indicated as dots. Right: fractional separation along the paths as a function of fractional path length.

Figure 1 illustrates an application of this methodology. Two planar PH quintic paths, of equal arc length S, are to be traversed at the same constant speed and a minimum safe separation of $0.025\,S$ is desired. Although these paths intersect twice, the computation with sampling distance $\Delta s = 0.005\,S$ indicates that the minimum separation has nevertheless been achieved. The method can be easily extended to spatial PH curves, and can also be adapted to accommodate variable speeds along the paths [13].

The use of *offset curves* to define "safety zones" of a specified width about the paths of multiple autonomous vehicles has also been proposed [27, 28, 29]. This is a conservative approach, that considers only the path geometry (not path timing) in maintaining safe vehicle separations: see Figure 2. PH curves have the advantage, in this context, that their offsets $\mathbf{r}_d(\xi) = \mathbf{r}(\xi) \pm d\,\mathbf{n}(\xi)$, where $\mathbf{n}(\xi)$ is the unit normal to $\mathbf{r}(\xi)$ and d is the offset distance, are *rational*

curves [16]: they admit parameterizations $\mathbf{r}_d(\xi) = (X(\xi)/W(\xi), Y(\xi)/W(\xi))$ where $W(\xi), X(\xi), Y(\xi)$ are relatively prime polynomials specifying the offset curve homogeneous coordinates. However, it should be noted that the offset curves illustrated in [27, 28, 29] are clearly incorrect.

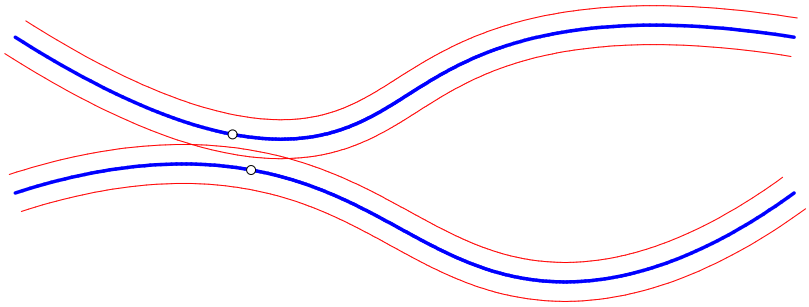

Figure 2: Two paths (blue) of identical arc length S with their offsets (red) at distance $\pm 0.025\, S$. Although the intersection of the offset curves indicates a potential violation of the prescribed minimum safe separation $\delta = 0.05\, S$, the actual points of closest approach (indicated by dots) are at distance $0.0515\, S$.

5 Simultaneous arrivals

Several authors have discussed the problem of ensuring simultaneous arrival of autonomous vechicles that follow different paths to a specified destination [5, 28, 29]. If the vehicles maintain the same constant speed, this amounts to designing smooth paths with different shapes but identical arc lengths. It has recently been demonstrated [11] that, for the case of planar PH quintic paths with different initial and final conditions, the requirement of equal arc lengths can be *exactly* achieved using a simple algorithm.

Consider the problem of constructing paths for the simultaneous arrival of vehicles with specified initial/final states travelling at constant speed (this may be considered a "strategic" path planning problem — it does not address short–term issues that may require communications between vehicles or path modification in real time). The construction of planar PH quintic paths with prescribed initial/final points $\mathbf{q}_0, \mathbf{q}_1$, tangents $\mathbf{t}_0, \mathbf{t}_1$, and arc length S may be summarized as follows (see [11] for complete details).

Using the complex representation with $\mathbf{q}_0 = x_0 + \mathrm{i}\, y_0$, $\mathbf{q}_1 = x_1 + \mathrm{i}\, y_1$ and $\mathbf{t}_0 = \exp(\mathrm{i}\,\theta_0)$, $\mathbf{t}_1 = \exp(\mathrm{i}\,\theta_1)$ and setting $\Delta\mathbf{q} = \mathbf{q}_1 - \mathbf{q}_0 := |\Delta\mathbf{q}| \exp(\mathrm{i}\,\alpha)$, the specified data is first reduced to canonical form by: (i) subtracting $\mathbf{q}_0$ from $\mathbf{q}_0$ and $\mathbf{q}_1$; (ii) dividing $\mathbf{q}_1$ by $\Delta\mathbf{q}$; (iii) multiplying $\mathbf{t}_0$ and $\mathbf{t}_1$ by $\exp(-\mathrm{i}\,\alpha)$; and (iv) dividing S by $|\Delta\mathbf{q}|$. This amounts to a translation/rotation/scaling transformation, that maps $\mathbf{q}_0$ and $\mathbf{q}_1$ to the points 0 and 1 on the real axis. Once the canonical form solution has been computed, it can be restored to the original coordinates by taking $\mathbf{p}_0 = \mathbf{q}_0$ in (5) and multiplying $\mathbf{w}_0, \mathbf{w}_1, \mathbf{w}_2$ by $\sqrt{|\Delta\mathbf{q}|} \exp(\mathrm{i}\,\frac{1}{2}\alpha)$ before substituting in (5). For brevity, only the generic case $\theta_1 \neq \pm\,\theta_0$ is considered here (see [11] for the special cases $\theta_1 = \pm\,\theta_0$).

For canonical form data, the coefficients of (2) are expressed as

$$\mathbf{w}_0 \;=\; w \exp(\mathrm{i}\tfrac{1}{2}\theta_0)\,, \quad \mathbf{w}_1 \;=\; u + \mathrm{i}\, v\,, \quad \mathbf{w}_2 \;=\; w \exp(\mathrm{i}\tfrac{1}{2}\theta_1)\,,$$

where the real unknowns u, v, w are determined as follows. First, setting

$$\begin{aligned} a_2 \;&=\; 2(c_0 s_1 - c_1 s_0)^2\,, \\ a_1 \;&=\; 3\,[\,2(c_0 c_1 + s_0 s_1 - 3)S + 3(c_0^2 - s_0^2 + c_1^2 - s_1^2) - 2(c_0 c_1 - s_0 s_1)\,]\,, \\ a_0 \;&=\; 36(S^2 - 1)\,, \end{aligned}$$

where $(c_0, s_0) := (\cos\frac{1}{2}\theta_0, \sin\frac{1}{2}\theta_0)$ and $(c_1, s_1) := (\cos\frac{1}{2}\theta_1, \sin\frac{1}{2}\theta_1)$, let

$$z \;=\; \frac{-\,a_1 - \sqrt{a_1^2 - 4a_2a_0}}{2a_2} \tag{10}$$

be the smaller root[2] of the equation $a_2z^2 + a_1z + a_0 = 0$, and set $w = \sqrt{z}$. Then, let $\mu, \nu = \pm 1$ be such that $\mu\nu$ and $(c_0s_1 + c_1s_0 - 3c_0s_0 - 3c_1s_1)z$ have the same sign. For each of the two μ, ν pairs thus identified, set

$$u \;=\; \frac{-3(c_0 + c_1)w + \mu\sqrt{p(z)}}{4} \quad \text{and} \quad v \;=\; \frac{-3(s_0 + s_1)w + \nu\sqrt{q(z)}}{4}\,, \tag{11}$$

where

$$p(z) \;=\; 60(S+1) - (15c_0^2 + 15c_1^2 - 10c_0c_1)z\,, \tag{12}$$

$$q(z) \;=\; 60(S-1) - (15s_0^2 + 15s_1^2 - 10s_0s_1)z\,. \tag{13}$$

In general, this yields two formal solutions to the problem of matching the given data, of which one has an attractive shape and the other exhibits an undesirable looping behavior — the latter can be identified and discarded by comparing the absolute rotation index for the two solutions (see Section 3).

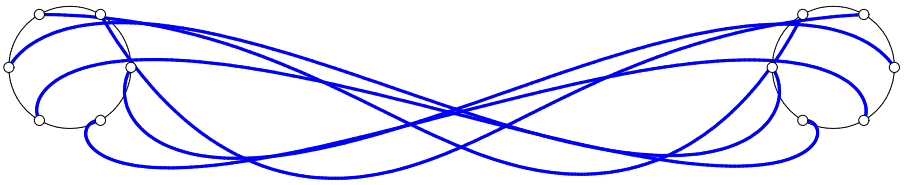

Figure 3: A family of simultaneous–arrival paths for a swarm of six unmanned constant speed vehicles, departing and arriving in different directions from a set of corresponding equidistant points on an initial and final target circle.

[2]It has been shown [11] that this equation always has two positive real roots, and the expressions (12) and (13) are both non–negative at the particular root (10).

Figure 3 shows a family of simultaneous–arrival paths for a swarm of six unmanned vehicles that start from equidistant points on an initial circle, and end at corresponding points on a target circle. The path length S is chosen to be 12.5% greater than the linear distance between the start and end points, and each vehicle has different departure/arrival directions. It is evident from Figure 4, which plots the 15 pair–wise separations (computed by the method described in Section 4), that a minimum safe separation equal to 1% of S is achieved despite the criss–cross nature of the different paths.

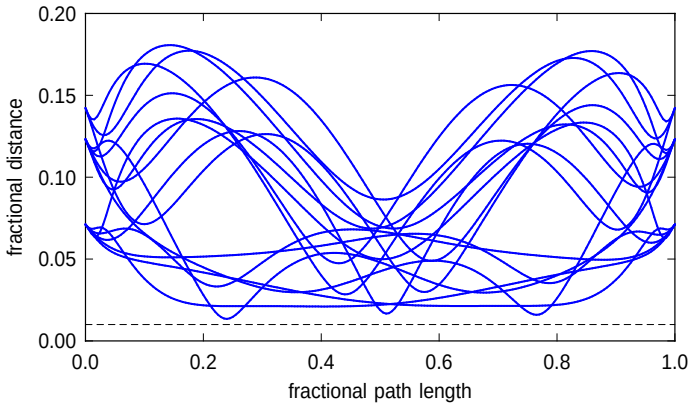

Figure 4: The 15 pair–wise separation plots for the six paths in Figure 3.

6 Curvature extrema of PH quintics

An unmanned vehicle can exert only a finite steering torque, which imposes an upper bound on the magnitude of feasible path curvatures [1, 4, 24, 27, 29]. Thus, the ability to identify the curvature extrema of PH curves is required, in order to ensure that prescribed curvature bounds are observed. From (4),

the curvature of a planar PH quintic has the form $\kappa(\xi) = h(\xi)/\sigma^2(\xi)$, where the quadratic polynomial $h(\xi)$ has the Bernstein coefficients

$$h_0 \;=\; 4\,\mathrm{Im}(\overline{\mathbf{w}}_0\mathbf{w}_1)\,, \quad h_1 \;=\; 2\,\mathrm{Im}(\overline{\mathbf{w}}_0\mathbf{w}_2)\,, \quad h_2 \;=\; 4\,\mathrm{Im}(\overline{\mathbf{w}}_1\mathbf{w}_2)\,. \tag{14}$$

Extrema of the curvature occur at the roots of its derivative,

$$\kappa'(\xi) \;=\; \frac{f(\xi)}{\sigma^3(\xi)}\,, \quad f(\xi) \;:=\; \sigma(\xi)h'(\xi) - 2\,h(\xi)\sigma'(\xi)\,.$$

The quintic polynomial $f(\xi)$ has the Bernstein coefficients

$$\begin{aligned}
f_0 \;&=\; 2\sigma_0 h_1 + 6\sigma_0 h_0 - 8\sigma_1 h_0\,,\\
f_1 \;&=\; (2\sigma_0 h_2 + 14\sigma_0 h_1 - 8\sigma_1 h_1 + 16\sigma_1 h_0 - 24\sigma_2 h_0)/5\,,\\
f_2 \;&=\; (4\,\sigma_0 h_2 + 20\sigma_1 h_1 - 18\sigma_2 h_1 + 6\sigma_2 h_0 - 12\sigma_3 h_0)/5\,,\\
f_3 \;&=\; (12\,\sigma_1 h_2 - 6\sigma_2 h_2 + 18\sigma_2 h_1 - 20\sigma_3 h_1 - 4\sigma_4 h_0)/5\,,\\
f_4 \;&=\; (24\sigma_2 h_2 - 16\sigma_3 h_2 + 8\sigma_3 h_1 - 14\sigma_4 h_1 - 2\sigma_4 h_0)/5\,,\\
f_5 \;&=\; 8\sigma_3 h_2 - 6\sigma_4 h_2 - 2\sigma_4 h_1\,,
\end{aligned}$$

and its real roots on the interval $\xi \in [\,0, 1\,]$ may be efficiently computed using the subdivision and variation–diminishing properties of the Bernstein form.

Prior studies [28] have suggested modifying the PH curve end derivative magnitudes as a means of subduing the extremum path curvature magnitude below a prescribed bound. However, no information is provided on how the extremal curvature is identified, and whether the prescribed curvature bound can always be satisfied by modifying the derivative magnitudes. Moreover, the plots in Figure 3 of [28] appear to be incorrect, since they indicate that curvature is non–differentiable at certain points along the paths.

Two methods for minimizing the maximum curvature magnitude $\kappa_{\max}$ of paths with prescribed end points and tangent directions are considered here.

In the first, the magnitudes $\ell_0 = |\mathbf{r}'(0)|$ and $\ell_1 = |\mathbf{r}'(1)|$ of the end derivatives are varied to obtain the (ℓ_0, ℓ_1) combination that gives the smallest $\kappa_{\max}$. The second employs the procedure described in Section 5 in constructing paths of increasing arc length S, to identify the value that yields the smallest $\kappa_{\max}$. Both methods use exact $\kappa_{\max}$ values, determined by comparing the values of $\kappa(\xi)$ at the roots $\xi \in (0,1)$ of the polynomial $f(\xi)$, and the interval end points $\xi = 0$ and 1. Both also impose an upper bound $S_{\max}$ on the allowed path arc length, since S should be reasonably commensurate with the linear distance between the path end points, and in some cases it may be possible to make $\kappa_{\max}$ very small by allowing S to become unreasonably large [3].

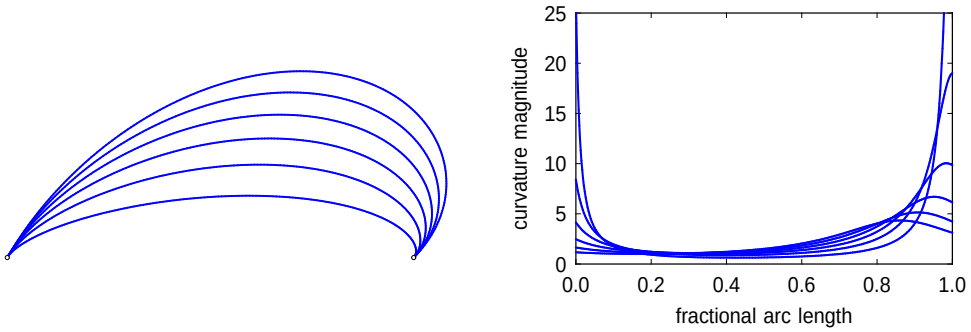

Figure 5: Left: A family of planar PH quintic interpolants to the end points $\mathbf{q}_0 = (0,0)$ and $\mathbf{q}_1 = (1,0)$ with tangent angles $\theta_0 = \pi/3$ and $\theta_1 = -3\pi/4$, for arc lengths $S = 1.1, \ldots, 1.6$. Right: curvature profiles for these interpolants.

Figure 5 shows interpolants to the end points $\mathbf{q}_0 = (0,0)$ and $\mathbf{q}_1 = (1,0)$ and end tangent directions $\theta_0 = \pi/3$, $\theta_1 = -3\pi/4$ for prescribed arc lengths $S = 1.1, \ldots, 1.6$, together with their curvature plots. For smaller values of S the extremal curvature occurs at an end point, but for larger values it is at an interior point. As seen in Figure 6, no minimum of $\kappa_{\max}$ exists for $S \leq 1.6$,

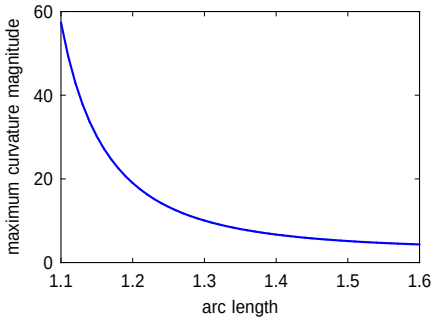

Figure 6: Maximum curvature magnitude versus arc length for paths with end points $\mathbf{q}_0 = (0,0)$, $\mathbf{q}_1 = (1,0)$ and tangent angles $\theta_0 = \pi/3$, $\theta_1 = -3\pi/4$.

and increasing S beyond ~ 1.3 yields only marginal reduction of $\kappa_{\max}$.

As an alternative to varying S, Figure 7 illustrates the effect of changing the end derivative magnitudes (for brevity, assumed equal) for interpolants to the end points $\mathbf{q}_0 = (0,0)$ and $\mathbf{q}_1 = (1,0)$ and tangent directions $\theta_0 = \pi/6$ and $\theta_1 = \pi/4$, using $\ell_0 = \ell_1 = 1.0, 1.5, \ldots, 4.0$. In this case, it is seen that the value of $\ell_0 = \ell_1$ has a strong influence on the nature of the curvature variation, and Figure 8 shows that the extremum curvature magnitude $\kappa_{\max}$ has a distinct minimum with respect to the magnitude of the end derivatives.

7 G^2 path corner rounding among obstacles

Another topic of considerable recent interest [20, 24, 27, 30] is path planning for autonomous vehicles that must navigate collision–free paths of bounded curvature through a field of obstacles. The classical problem of constructing a planar path of minimum length through a field of polygonal obstacles is considered here. At present, only the case of static obstacles is addressed, and

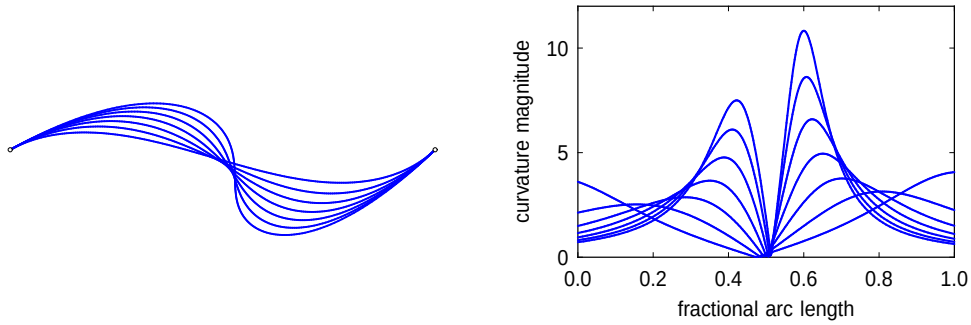

Figure 7: Left: Planar PH quintic interpolants to end points $\mathbf{q}_0 = (0, 0)$ and $\mathbf{q}_1 = (1, 0)$ with tangent angles $\theta_0 = \pi/6$, $\theta_1 = \pi/4$ and derivative magnitudes $\ell_0 = \ell_1 = 1.0, 1.5, \ldots, 4.0$. Right: the curvature plots for these interpolants.

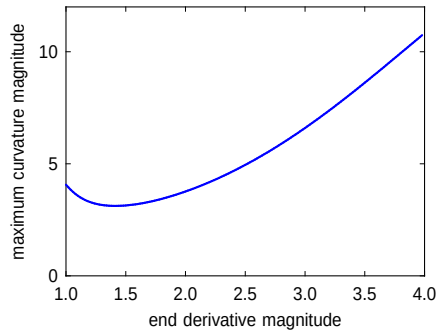

Figure 8: Largest curvature magnitude versus end derivative magnitude for paths from $\mathbf{q}_0 = (0, 0)$ to $\mathbf{q}_1 = (1, 0)$ and tangent angles $\theta_0 = \pi/6$, $\theta_1 = \pi/4$.

the vehicle is assumed to be of negligible size compared to the obstacles. This may be considered an "off–line" path planning problem, that is dependent on complete *a priori* knowledge of the obstacle field. The problem of "on–line" path planning, which may employ real–time vehicle sensing and control to accommodate a changing environment, is not addressed herein.

Since the theoretical minimum–length path through a polygonal obstacle field is piecewise–linear, it is incompatible with path curvature constraints imposed by vehicle steering mechanisms. It is shown that planar PH quintic segments can be employed to "round" the sharp corners of optimal piecewise–linear paths in a curvature–continuous manner, that guarantees satisfaction of both the obstacle avoidance and curvature bound constraints.

The solution to the basic path planning problem is based on constructing a visibility graph, and using standard algorithms to identify the shortest path between two graph vertices. In [19] this method was modified to replace the linear path segments by a G^1 sequence of PH quintics. The aim of the present approach is to retain the piecewise–linear solution, as far as possible, but to "round" its sharp corners using PH quintics meeting the linear segments with G^2 continuity. The obstacles are first offset[3] by a distance d, to be determined so as to ensure satisfaction of the obstacle avoidance and extremum curvature constraints. The optimal piecewise–linear path through these offset obstacles is then computed by means of the standard algorithms.

Consider the rounding of two line segments meeting at a corner point $\mathbf{p}_c$.

[3]For simplicity, a "polygonal" offset is used, without circular fillets at the sharp corners: the obstacle avoidance constraint is nevertheless exactly observed. Note that the obstacle offset is not required by the method in [19] if the vehicle is of negligible size.

The sharp corner is to be replaced by a PH quintic $\mathbf{r}(\xi)$, $\xi \in [\,0,1\,]$ starting at a point $\mathbf{r}(0) = \mathbf{p}_i$ on the incoming segment, and ending at a point $\mathbf{r}(1) = \mathbf{p}_o$ on the outgoing segment, where $|\mathbf{p}_c - \mathbf{p}_i| = |\mathbf{p}_o - \mathbf{p}_c|$ ($= L$, say). To ensure a G^2 rounded corner, the end tangents $\mathbf{t}(0)$ and $\mathbf{t}(1)$ should be parallel to $\mathbf{p}_c - \mathbf{p}_i$ and $\mathbf{p}_o - \mathbf{p}_c$, and the end curvatures must satisfy $\kappa(0) = \kappa(1) = 0$. It is convenient consider data in the canonical form[4]

$$\mathbf{p}_i \;=\; (0,0)\,, \quad \mathbf{p}_c \;=\; (L,0)\,, \quad \mathbf{p}_o \;=\; ((1+\cos\theta)L, \sin\theta\, L)\,,$$

the "turning angle" θ being measured positive anti–clockwise (see Figure 9). The solution for general data $\mathbf{p}_i, \mathbf{p}_c, \mathbf{p}_o$ is then obtained [15] by taking $\mathbf{p}_0 = \mathbf{p}_i$ in (5), and multiplying the coefficients $\mathbf{w}_0, \mathbf{w}_1, \mathbf{w}_2$ of (2) by $\exp(\mathrm{i}\frac{1}{2}\phi)$ where, writing $\mathbf{p}_i = (x_i, y_i)$ and $\mathbf{p}_c = (x_c, y_c)$, the angle ϕ is determined from

$$\cos\phi \;=\; \frac{x_c - x_i}{|\mathbf{p}_c - \mathbf{p}_i|}\,, \quad \sin\phi \;=\; \frac{y_c - y_i}{|\mathbf{p}_c - \mathbf{p}_i|}\,.$$

The solution for canonical–form data is defined (see [15] for complete details) in terms of L and θ by

$$\mathbf{w}_0 \;=\; \lambda\sqrt{L}\,, \quad \mathbf{w}_1 \;=\; 0\,, \quad \mathbf{w}_2 \;=\; \lambda\sqrt{L}\,\exp(\mathrm{i}\tfrac{1}{2}\theta)\,, \tag{15}$$

where

$$\lambda \;=\; \sqrt{30\cos\tfrac{1}{2}\theta/(6\cos\tfrac{1}{2}\theta + 1)}\,.$$

The control points of $\mathbf{r}(\xi)$ are obtained from (5). Note that $\mathbf{p}_2 = \mathbf{p}_1$ and $\mathbf{p}_4 = \mathbf{p}_3$, since $\mathbf{w}_1 = 0$, so the G^2 PH quintic corner curves have just four distinct control points [8] — examples are illustrated in Figure 9.

[4]The canonical form employed here is somewhat different from that used in Section 5, in the context of paths with equal arc lengths.

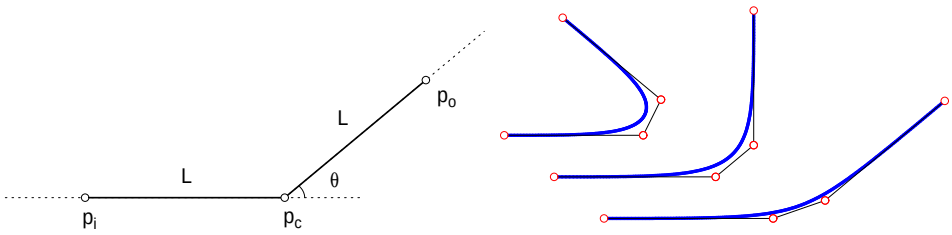

Figure 9: Left: canonical data defining a G^2 PH quintic corner curve. Right: examples of PH quintic corner curves for turning angles $\theta = 45°, 90°, 135°$.

The parametric speed (6) of the corner curve has the Bernstein coefficients

$$\sigma_0 = \lambda^2 L\,, \quad \sigma_1 = 0\,, \quad \sigma_2 = \frac{\lambda^2 L \cos\frac{1}{2}\theta}{3}\,, \quad \sigma_3 = 0\,, \quad \sigma_4 = \lambda^2 L\,,$$

and the curvature can be expressed as

$$\kappa(\xi) \;=\; 4\,\lambda^2 L \sin\tfrac{1}{2}\theta\,\frac{(1-\xi)\xi}{\sigma^2(\xi)}\,. \tag{16}$$

The extremum curvature $\kappa_e = \kappa(\frac{1}{2})$ and total arc length S are given [15] by

$$\kappa_e \;=\; \frac{32(6\cos\frac{1}{2}\theta + 1)\tan\frac{1}{2}\theta}{15L(\cos\frac{1}{2}\theta + 1)^2} \quad \text{and} \quad S \;=\; \frac{2L(6+\cos\frac{1}{2}\theta)\cos\frac{1}{2}\theta}{6\cos\frac{1}{2}\theta + 1}\,. \tag{17}$$

Finally, the deviation of the mid–point $\mathbf{r}(\frac{1}{2})$ from the corner point $\mathbf{p}_c$ is

$$\delta \;=\; \frac{(3\cos\frac{1}{2}\theta + 8)\,|\sin\frac{1}{2}\theta\,|\,L}{8(6\cos\frac{1}{2}\theta + 1)}\,. \tag{18}$$

Since θ is fixed by the corner geometry, the parameter L should be used to adjust the extremum curvature κ_e and deviation δ.

For the (non–rounded) offset at distance d to a convex polygonal obstacle, the offset point to a vertex with a turning angle θ is distance $d\sec\frac{1}{2}\theta$ from that vertex, and to prevent intrusion of the corner rounding curve within the

obstacle, this must exceed the value (18) — i.e.,

$$d \sec \tfrac{1}{2}\theta \; > \; \frac{(3 \cos \tfrac{1}{2}\theta + 8) \, |\sin \tfrac{1}{2}\theta \,| \, L}{8(6 \cos \tfrac{1}{2}\theta + 1)} \, ,$$

or equivalently

$$L \; < \; L_{\max} \; := \; \frac{8(6 + \sec \tfrac{1}{2}\theta) \, d}{(3 \cos \tfrac{1}{2}\theta + 8) \, |\sin \tfrac{1}{2}\theta \,|} \, . \tag{19}$$

Now if $\kappa_{\max}$ is the maximum allowed magnitude of path curvature, and $r_{\min} = 1/\kappa_{\max}$ is the minimum radius of curvature, from (17) the condition $|\kappa_e| < \kappa_{\max}$ becomes

$$\frac{32(6 \cos \tfrac{1}{2}\theta + 1) |\tan \tfrac{1}{2}\theta \,|}{15 L (\cos \tfrac{1}{2}\theta + 1)^2} \; < \; \frac{1}{r_{\min}} \, ,$$

or equivalently

$$L \; > \; L_{\min} \; := \; \frac{32(6 \cos \tfrac{1}{2}\theta + 1) |\tan \tfrac{1}{2}\theta| \; r_{\min}}{15(\cos \tfrac{1}{2}\theta + 1)^2} \, . \tag{20}$$

If the bounds (19) and (20) on L are to be compatible, the condition

$$\frac{8(6 + \sec \tfrac{1}{2}\theta) \, d}{(3 \cos \tfrac{1}{2}\theta + 8) \, |\sin \tfrac{1}{2}\theta \,|} \; > \; \frac{32(6 \cos \tfrac{1}{2}\theta + 1) |\tan \tfrac{1}{2}\theta \,| \, r_{\min}}{15(\cos \tfrac{1}{2}\theta + 1)^2} \, ,$$

must be satisfied, and this can be reduced to

$$d \; > \; \frac{4(3 \cos \tfrac{1}{2}\theta + 8) \sin^2 \tfrac{1}{2}\theta}{15(\cos \tfrac{1}{2}\theta + 1)^2} \; r_{\min} \, . \tag{21}$$

The factor multiplying $r_{\min}$ on the right is monotonically increasing with $|\theta|$, from 0 when $\theta = 0$ to 32/15 when $\theta = \pm\pi$. If $r_{\min}$ is specified *a priori*, and the largest turning angle magnitude $\theta_{\max}$ is identified, substituting it in (21) determines the minimum offset distance $d_{\min}$ ensuring satisfaction of both the maximum path curvature and obstacle non–intrusion conditions.

With $d = d_{\min}$, one has $L_{\min} = L_{\max}$ at the corner(s) for which $|\theta| = \theta_{\max}$, and the particular value $L = L_{\min} = L_{\max}$ must be used. At the other corners,

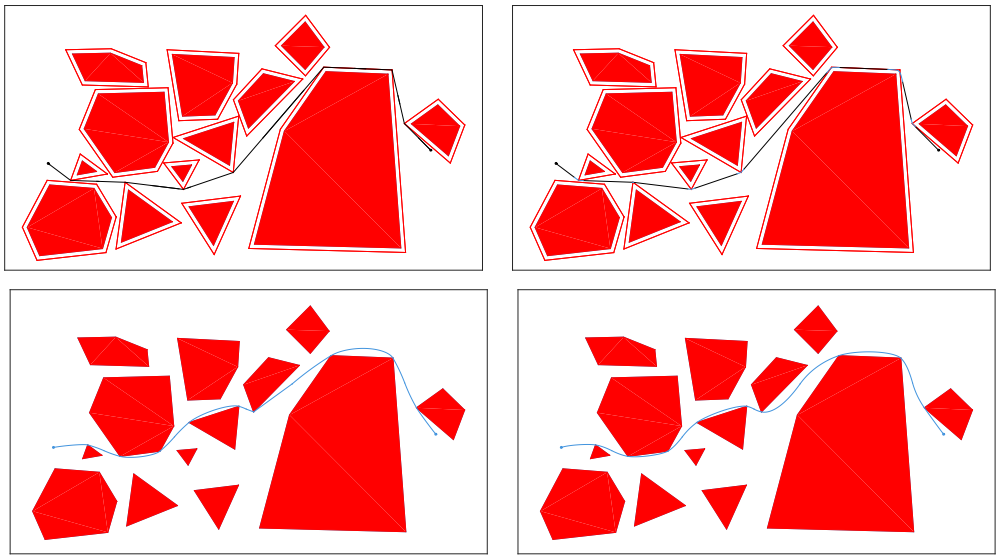

Figure 10: Top: piecewise–linear path among a field of offset obstacles (left) and this path with G^2 PH quintic rounded corners (right). Bottom: G^1 PH quintic paths with tangents defined by the T1 (left) and T2 (right) method.

it may be possible to use larger values of L, but the sum of the L values for two consecutive corners cannot exceed the linear path length between them. Thus, for small and closely–spaced obstacles, it may not be possible to satisfy both the collision avoidance and curvature bound constraints.

Figure 10 shows the nominal piecewise–linear path among a field of offset obstacles, and this path with G^2 PH quintic rounded corners using $d = 0.2136$ and the curvature bound $|\kappa| \leq 5$. Also shown are two paths specified by G^1 PH quintic segments, that do not require obstacles offsets and use different strategies for assigning the nodal tangents [19] — the T1 method employs a weighted average of successive linear displacement vectors and the T2 method uses tangents obtained from a C^2 PH quintic spline fit [12]. The piecewise–linear path with G^2 rounded corners has an overall length 23.8254, somewhat less than the value 23.9394 for the sharp–corner path. Note that the two G^1 piecewise PH quintic paths take a different route through the obstacle field, and have larger overall lengths — namely, 25.6534 using the T1 method for assigning nodal tangents, and 25.3819 using the T2 method.

Figure 11 compares curvature plots for the G^2 rounded–corner path and the two G^1 paths. The former evidently attains the curvature bound $\kappa_{\max} = 5$ around each corner. Using the T1 tangent assignment method, the G^1 path clearly exceeds this bound, and exhibits large curvature discontinuities. With the T2 tangent method, the curvature extrema are substantially suppressed, although significant path curvature discontinuites are still evident.

A more intricate example is shown in Figure 12, involving a path through a single polygonal obstacle with many convex and concave corners, using the values $d = 0.1736$ and $\kappa_{\max} = 5$. The piecewise–linear path involves 14 sharp

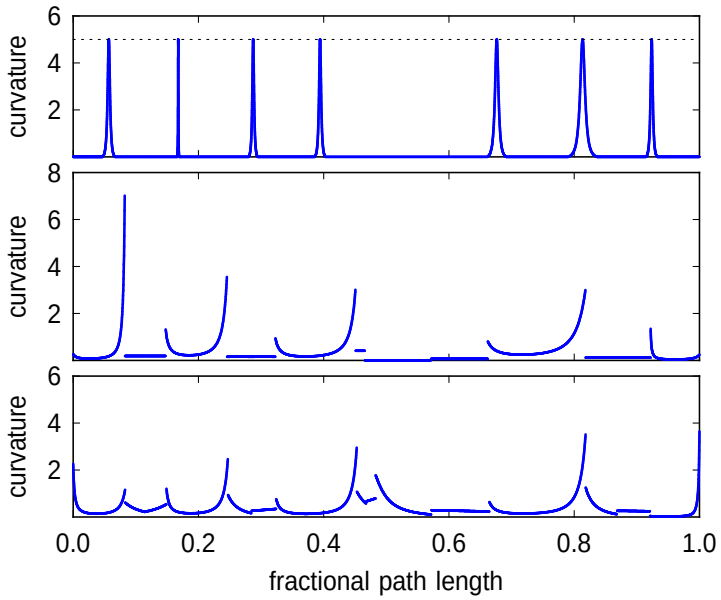

Figure 11: Upper: curvature magnitude for the piecewise–linear path with G^2 PH quintic rounded corners, showing the curvature bound $|\kappa| \leq 5$. Also shown are curvature magnitudes for the G^1 piecewise PH quintic paths with nodal tangents defined by the T1 method (center) and T2 method (lower).

corners, and in every case the G^2 PH quintic corner rounding curves avoid obstacle encroachment and exactly attain the specified curvature bound.

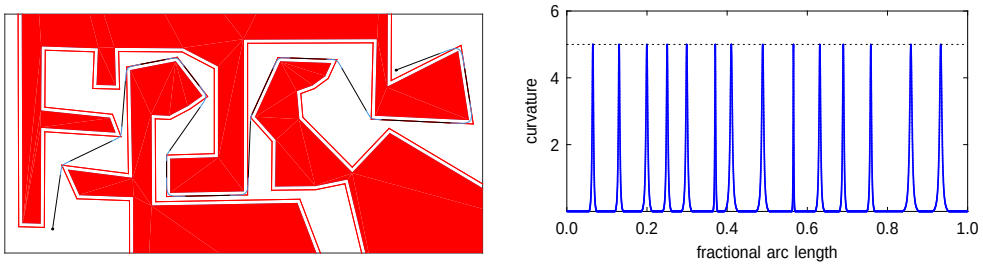

Figure 12: Left: piecewise–linear path through a single intricate obstacle with sharp corners rounded by G^2 PH quintic segments that satisfy the curvature bound $|\kappa| \leq 5$. Right: variation of the curvature magnitude along this path.

The examples shown in Figures 10 and 12 employ the value $L_{\min}$ defined by (20) at each corner, so the corner curves are of minimun size and attain the prescribed curvature magnitude bound $\kappa_{\max}$. Using larger L values yields lower corner curvatures, and somewhat smaller total path lengths. However, L values smaller than $L_{\max}$ defined by (19) are generally necessary, to avoid any overlap of consecutive corner curves. Figure 13 compares the path and curvature distribution for the $L = L_{\min}$ case in Figure 10 with a case in which L is as large as possible for each corner, without overlap of the corner curves (the path still avoid encroachment on any of the obstacles). The use of larger L values evidently yields smaller peak curvature magnitudes, and the overall arc length is slightly reduced, from $S = 23.8254$ to $S = 23.5836$.

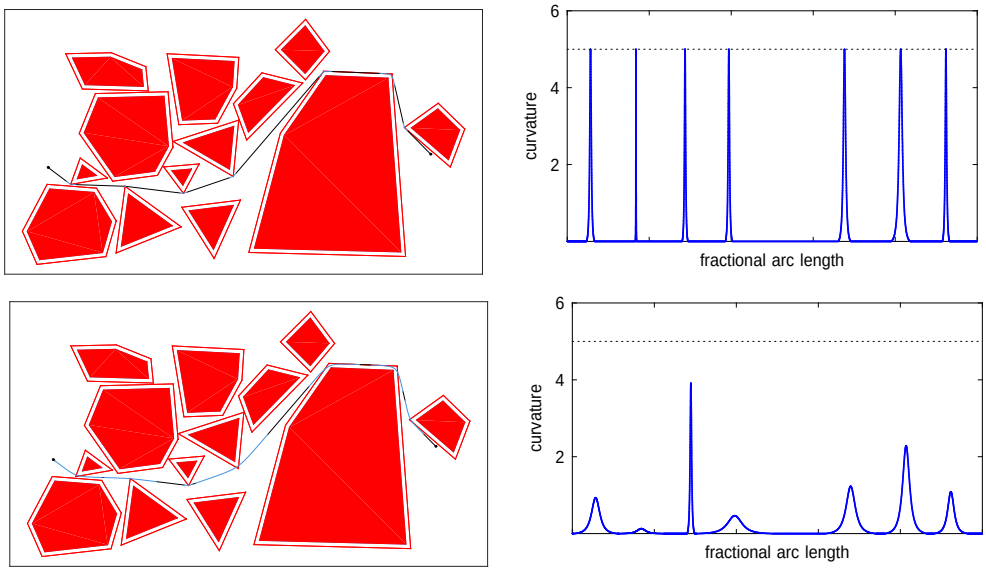

Figure 13: Paths and curvature plots for the obstacle field in Figure 10 using PH corner curves of minimum size $L_{\min}$ in each case (upper), and the largest size L in each case that does not incur overlap of the corner curves (lower).

8 Closure

Exploiting the distinctive properties of Pythagorean–hodograph (PH) curves, a number of basic utilities have been presented in this paper that are useful in path planning for unmanned or autonomous air, ground, or undersea vehicles. Instead of addressing a specific path planning scenario in detail, the emphasis herein has been to provide a family of rigorous, broadly applicable, and easily implemented functions, and also to address pervasive misconceptions in prior studies concerning the basic properties and capabilities of PH curves.

The problems treated in this study include: (1) maintenance of minimum safe separations between vehicles that execute different paths at a fixed speed; (2) design of curved paths with identical arc lengths, ensuring simultaneous arrival at fixed speed; (3) path curvature minimization, subject to maximum path length, to ensure compatibility with vehicle steering constraints; and (4) curvature–continouous corner rounding of shortest paths through polygonal obstacle fields, consistent with a prescribed maximum path curvature.

For brevity, the focus of this study has been on planar PH paths and the complex representation has been extensively used. Although the quaternion representation for spatial PH curves is more involved, many of the procedures readily extend to three–dimensional paths. Another topic deserving further investigation is the capability of PH paths to accommodate continuously–variable path speeds, specified as functions of the elapsed time, path length travelled, path curvature, or other variables of interest.

References

[1] G. Ambrosino, M. Arioloa, U. Ciniglio, F. Corraro, E. De Lellis, and A. Pironti (2009), Path generation and tracking in 3D for UAVs, *IEEE Trans. Contr. Syst. Technol.* **17**, 980–988.

[2] A. Askari, M. Mortazavi, H. A. Talebi, and A. Motamedi (2016), A new approach in UAV path planning using Bézier–Dubins continuous curvature path, *J. Aerosp. Eng.* **230**, 1103–1113.

[3] G. Birkhoff and C. de Boor (1965), Piecewise polynomial interpolation and approximation, in *Approximation of Functions* (H. L. Garabedian, ed.), Elsevier, Amsterdam, 164–190.

[4] H. Bruyninckx and D. Reynaerts (1997), Path planning for mobile and hyper–redundant robots using Pythagorean–hodograph curves, *Proceedings, International Conference on Advanced Robotics* (ICAR 97), Monterey, CA, 595–600.

[5] R. Choe, V. Cichella, E. Xargay, N. Hovakimyan, A. C. Trujillo, and I. Kaminer (2013), A trajectory–generation framework for time–critical cooperative missions, *Proceedings, AIAA Infotech Aerospace Conference*, Boston, MA.

[6] K. Chu, J. Kim, K. Jo, and M. Sunwoo (2015), Real–time path planning of autonomous vehicles for unstructured road navigation, *Int. J. Automot. Technol.* **16**, 653–668.

[7] B. Dong and R. T. Farouki (2015), Algorithm 952: `PHquintic`: A library of basic functions for the construction and analysis of planar quintic Pythagorean–hodograph curves, *ACM Trans. Math. Software* **41** (4), Article 28.

[8] R. T. Farouki (1994), The conformal map $z \rightarrow z^2$ of the hodograph plane, *Comput. Aided Geom. Design* **11**, 363–390.

[9] R. T. Farouki (1996), The elastic bending energy of Pythagorean–hodograph curves, *Comput. Aided Geom. Design* **13**, 227–241.

[10] R. T. Farouki (2008), *Pythagorean–Hodograph Curves: Algebra and Geometry Inseparable*, Springer, Berlin.

[11] R. T. Farouki (2016), Construction of G^1 planar Hermite interpolants with prescribed arc lengths, *Comput. Aided Geom. Design* **46**, 64–75.

[12] R. T. Farouki, B. K. Kuspa, C. Manni, and A. Sestini (2001), Efficient solution of the complex quadratic tridiagonal system for C^2 PH quintic splines, *Numer. Algor.* **27**, 35–60.

[13] R. T. Farouki, J. Manjunathaiah, and G–F. Yuan (1999), G codes for the specification of Pythagorean–hodograph tool paths and associated feedrate functions on open–architecture CNC machines, *Inter. J. Mach. Tools Manuf.* **39**, 123–142.

[14] R. T. Farouki and C. A. Neff (1995), Hermite interpolation by Pythagorean–hodograph quintics, *Math. Comp.* **64**, 1589–1609.

[15] R. T. Farouki and K. M. Nittler (2016), Efficient high–speed cornering motions based on continuously–variable feedrates I. Real–time interpolator algorithms, *Int. J. Adv. Manuf. Technol.* to appear.

[16] R. T. Farouki and T. Sakkalis (1990), Pythagorean hodographs, *IBM J. Res. Develop.* **34**, 736–752.

[17] R. T. Farouki and T. Sakkalis (1991), Real rational curves are not "unit speed," *Comput. Aided Geom. Design* **8**, 151–157.

[18] D. de A. Fernandes, A. J. Sørensen, and D. C. Donha (2013), Path generation for high–performance motion of ROVs based on a reference model, *Model. Ident. Control* **36**, 81–101.

[19] C. Giannelli, D. Mugnaini, and A. Sestini (2016), Path planning with obstacle avoidance by G^1 PH quintic splines, *Comput. Aided Design* **75-76**, 47–60.

[20] D. G. Macharet, A. A. Neto, and M. F. M. Campos (2009), On the generation of feasible paths for aerial robots in environments with obstacles, *Proceedings, 2009 IEEE/RSJ International Conference on Intelligent Robots and Systems*, Saint Louis, MO, 3380–3385.

[21] A. A. Neto and M. F. M. Campos (2009), A path planning algorithm for UAVs with limited climb angle, *Proceedings, 2009 IEEE/RSJ International Conference on Intelligent Robots and Systems*, Saint Louis, MO, 3894–3899.

[22] A. A. Neto and M. F. M. Campos (2009), On the generation of feasible paths for aerial robots with limited climb angle, *Proceedings, 2009*

IEEE International Conference on Robotics and Automation, Kobe, Japan, 2872–2877.

[23] A. A. Neto, D. G. Macharet, and M. F. M. Campos (2010), Feasible RRT–based path planning using seventh order Bézier curves, *Proceedings, 2010 IEEE/RSJ International Conference on Intelligent Robots and Systems*, Taipei, Taiwan, 1445–1450.

[24] A. A. Neto, D. G. Macharet, and M. F. M. Campos (2010), On the generation of trajectories for multiple UAVs in environments with obstacles, *J. Intell. Robot Syst.* **57**, 123–141.

[25] A. A. Neto, D. G. Macharet, and M. F. M. Campos (2013), Feasible path planning for fixed–wing UAVs using seventh order Bézier curves, *J. Braz. Comput. Soc.* **19**, 193–203.

[26] A. A. Neto, D. G. Macharet, and M. F. M. Campos (2015), 3D path planning with continuous bounded curvature and pitch angle profiles using 7th order curves, *Proceedings, 2015 IEEE/RSJ International Conference on Intelligent Robots and Systems* (IROS), Hamburg, Germany, 4923–4928.

[27] M. Shanmugavel, A. Tsourdos, R. Zbikowski, and B. White (2005), Path planning of multiple UAVs in an environment of restricted regions, *Proceedings, 2005 ASME International Mechanical Engineering Congress and Exposition* (IMECE2005), Orlando, FL, IMECE2005–79682.

[28] M. Shanmugavel, A. Tsourdos, R. Zbikowski, B. A. White, C. A. Rabbath, and N. Léchevin (2006), A solution to simultaneous arrival of multiple UAVs using Pythagorean hodograph curves, *Proceedings, 2006 American Control Conference*, 2813–2818.

[29] M. Shanmugavel, A. Tsourdos, B. A. White, and R. Zbikowski (2007), Differential geometric path plannings of multiple UAVs, *ASME J. Dyn. Syst. Meas. Control* **129**, 620–632.

[30] M. Shanmugavel, A. Tsourdos, and B. A. White (2010), Collision avoidance and path planning of multiple UAVs using flyable paths in 3D, *Proceedings, 15th International Conference on Methods and Models in Automation and Robotics* (MMAR), Miedzyzdroje, Poland, 218–222.

[31] S. Subchan, B. A. White, A. Tsourdos, M. Shanmugavel, and R. Zbikowski (2008), Pythagorean hodograph (PH) planning for tracking airborne contaminant using sensor swarm, *Proceedings, IEEE International Instrumentation and Measurement Control Technology Conference* (I^2MTC 2008).

List of figure captions

Figure 1. Left: two planar PH quintic paths of equal arc length traversed at constant speed, with the points of closest approach indicated as dots. Right: fractional separation along the paths as a function of fractional path length.

Figure 2. Two paths (blue) of identical arc length S with their offsets (red) at distance $\pm 0.025\, S$. Although the intersection of the offset curves indicates a potential violation of the prescribed minimum safe separation $\delta = 0.05\, S$, the actual points of closest approach (indicated by dots) are at distance $0.0515\, S$.

Figure 3. A family of simultaneous–arrival paths for a swarm of six unmanned constant speed vehicles, departing and arriving in different directions from a set of corresponding equidistant points on an initial and final target circle.

Figure 4. The 15 pair–wise separation plots for the six paths in Figure 3.

Figure 5. Left: A family of planar PH quintic interpolants to the end points $\mathbf{q}_0 = (0, 0)$ and $\mathbf{q}_1 = (1, 0)$ with tangent angles $\theta_0 = \pi/3$ and $\theta_1 = -3\pi/4$, for arc lengths $S = 1.1, \ldots, 1.6$. Right: curvature profiles for these interpolants.

Figure 6. Maximum curvature magnitude versus arc length for paths with end points $\mathbf{q}_0 = (0, 0)$, $\mathbf{q}_1 = (1, 0)$ and tangent angles $\theta_0 = \pi/3$, $\theta_1 = -3\pi/4$.

Figure 7. Left: Planar PH quintic interpolants to end points $\mathbf{q}_0 = (0, 0)$ and $\mathbf{q}_1 = (1, 0)$ with tangent angles $\theta_0 = \pi/6$, $\theta_1 = \pi/4$ and derivative magnitudes $\ell_0 = \ell_1 = 1.0, 1.5, \ldots, 4.0$. Right: the curvature plots for these interpolants.

Figure 8. Largest curvature magnitude versus end derivative magnitude for paths from $\mathbf{q}_0 = (0, 0)$ to $\mathbf{q}_1 = (1, 0)$ and tangent angles $\theta_0 = \pi/6$, $\theta_1 = \pi/4$.

Figure 9. Left: canonical data defining a G^2 PH quintic corner curve. Right: examples of PH quintic corner curves for turning angles $\theta = 45°$, $90°$, $135°$.

Figure 10. Top: piecewise–linear path among a field of offset obstacles (left) and this path with G^2 PH quintic rounded corners (right). Bottom: G^1 PH quintic paths with tangents defined by the T1 (left) and T2 (right) method.

Figure 11. Upper: curvature magnitude for the piecewise–linear path with G^2 PH quintic rounded corners, showing the curvature bound $|\kappa| \leq 5$. Also shown are curvature magnitudes for the G^1 piecewise PH quintic paths with nodal tangents defined by the T1 method (center) and T2 method (lower).

Figure 12. Left: piecewise–linear path through a single intricate obstacle with sharp corners rounded by G^2 PH quintic segments that satisfy the curvature bound $|\kappa| \leq 5$. Right: variation of the curvature magnitude along this path.

Figure 13. Paths and curvature plots for the obstacle field in Figure 10 using PH corner curves of minimum size $L_{\min}$ in each case (upper), and the largest size L in each case that does not incur overlap of the corner curves (lower).

d	distance
f, h	real values
j, k, m	integers
n	curve degree
p, q	real values
r	radius of curvature
s	arc length
t	time
u, v	real values
x, y	Cartesian coordinates
L	corner curve dimension
V	speed
S	total arc length
W, X, Y	homogeneous coordinates
$\mathbf{n}$	curve normal
$\mathbf{p}, \mathbf{q}, \mathbf{r}, \mathbf{s}$	position vectors
$\mathbf{t}$	curve tangent
$\mathbf{w}$	complex number
δ	minimum distance
θ	tangent angle/corner angle
κ	curvature
μ, ν, ξ	curve parameter
σ	parametric speed
$\Delta\mathbf{q}$	displacement vector
Δs	arc length increment
Δt	sampling time

Table 1: List of notations